Propagation of transverse optical coherence in random multiple-scattering media

Chung-Chieh Cheng and M. G. Raymer
Oregon Center for Optics and Department of Physics, University of Oregon, Eugene, Oregon 97403
(Received 6 March 2000; published 19 July 2000)

We experimentally investigate the evolution of the transverse spatial coherence of light as it traverses a random, multiple-scattering medium. For near-forward scattering, it has been proposed that the wave-transport process can be well described by a transport equation for the spatial-angular Wigner function of the light, or equivalently for the two-point spatial coherence function (mutual intensity). We find good agreement between the wave-transport theory and our experimental results for media of different thickness. In a dense medium (for example, optical distance, or density, greater than 5), the nature of the scattered light field can be qualitatively described by a complex Gaussian-Schell model, which raises an interesting interpretation about the process of long-path optical transport.

PACS number(s): 42.50.Ar, 42.25.Dd, 42.25.Kb

I. INTRODUCTION

Light transport in random, multiple-scattering media has a wide range of applications in biomedical imaging [1], astronomy [2], illuminating engineering [3], and geophysics [4]. Radiative transfer, a widely used model for light transport, is based on a Boltzmann-type equation describing the evolution of the radiance, or specific intensity [2–5]. This energy-transport model neglects the wave nature of light, so it is limited to describing incoherent light only. In some instances this model may be an adequate description. However, light has an intrinsic wave nature, and often this strongly influences light transport as a consequence of diffraction and interference [6]. To include wave aspects of partially coherent light, efforts have been made to generalize the theory of radiative transfer. In the case of free-space transport, the generalized radiance was introduced to replace the radiance as the fundamental quantity that is transported [7].

In the case of transport in a random, multiply scattering medium, there are many situations in which the key quantity of interest to experimenters is the specific intensity, since it can be measured rather easily. Nevertheless, as we demonstrate here, in order to obtain a more quantitative understanding of transport, both theoretically and experimentally, one should go beyond this lowest-order, incoherent description of light. In principle, one should consider a hierarchy of higher-order, multipoint correlation functions of the field. In this context, recent work has focused on such subtle issues as coherent backscattering, light localization, and non-Gaussian intensity statistics [8]. A general theory describing these effects involves tracking an essentially infinite number of higher-order field correlation functions as the light propagates. This makes such an approach intractable for use in modeling transport in realistic systems of practical interest, which are often complex and inhomogeneous.

The question we address in this study is whether there exists an intermediate level of description that lies between the overly simplified, conventional transport theory and the modern, field-theoretic treatments [8] that come with great complexity. Encouragingly, we verify by experiments and modeling that such a level does exist in the regime dominated by near-forward scattering. We find that a formalism [1,9] based on the two-point spatial coherence function (or the related Wigner distribution function) provides a self-consistent description of wave transport that is subject to direct experimental verification.

The spatial coherence function (SCF) (also called the mutual intensity) of light is defined as

$$\rho(\vec{r}_1,\vec{r}_2,t)=\langle E(\vec{r}_1;t)E^*(\vec{r}_2;t)\rangle, \tag{1}$$

where $\vec{r}_1$ and $\vec{r}_2$ are position vectors, and $E(\vec{r};t)$ is the complex, scalar electric field. The bracket indicates an ensemble average over all possible realizations of $E(\vec{r};t)$, each being associated with a particular configuration of the medium, which is subject to spatial and/or temporal fluctuations. From elementary classical coherence theory it is well known that the SCF manifests the second-order spatial coherence property of light [5]. Importantly, the SCF can be measured by interferometry [10] or by phase-space tomography [11]. Within the range of experimental parameters considered (corresponding to predominantly near-forward scattering), our measurements of the two-point spatial coherence function are found to be in good quantitative agreement with the predictions of a wave-transport model for the Wigner function.

In this paper we first review a recently proposed transport equation for the Wigner function, and its solution in the case of near-forward scattering. Then we present the results of measurements of the SCF and Wigner function for light after traversing a medium of polystyrene microspheres in a gelatin medium. After a comparison between the experimental results and the theoretical predictions, we develop a simplified analytical approach to solving the Wigner-function transport equation. The form of the solution found here demonstrates the connection between the transport problem and the Gaussian-Schell model for partially coherent light [5]. In particular, we find that in a dense medium an initially coherent beam is transformed into a complex Gaussian-Schell source, to a good approximation. This allows also a connection to be made between the transport equation and a simplified version based on a Fokker-Planck equation.

Another application for theories of random light propagation is in the case of light in a turbulent atmosphere. In this context, which is dominated by near-forward scattering, a formalism has been based on the paraxial approximation, and is known as the extended Huygens-Fresnel formalism (EHF) [12,13]. We show that the wave-transport equation that we use is equivalent to the EHF in the case of near-forward scattering, which is the region in which our experiments are carried out.

II. WAVE TRANSPORT EQUATION

For a beam propagating in the z direction, the transverse Wigner function (WF) of light may be defined as

$$W(\vec{x}_\perp,\vec{k}_\perp,z;t)=\int \frac{d^2\vec{s}_\perp}{(2\pi)^2}\exp[-i\vec{s}_\perp\cdot\vec{k}_\perp] \times\rho(\vec{x}_\perp+\vec{s}_\perp/2,\vec{x}_\perp-\vec{s}_\perp/2,z;t), \tag{2}$$

where

$$\rho(\vec{x}_\perp+\vec{s}_\perp/2,\vec{x}_\perp-\vec{s}_\perp/2,z;t) =\langle E(\vec{x}_\perp+\vec{s}_\perp/2,z;t)E^*(\vec{x}_\perp-\vec{s}_\perp/2,z;t)\rangle \tag{3}$$

is the transverse spatial coherence function of light, $\vec{x}_\perp=(x,y,0)$, and $\vec{s}_\perp=(s_x,s_y,0)$. It has been proposed that the WF of light traversing a homogeneous medium with a random distribution of scatterers obeys a Boltzmann-type transport equation [9,14,15,16]

$$\left(\partial_t+v\partial_z+\frac{v}{k}\vec{k}_\perp\cdot\vec{\nabla}_{\vec{x}\perp}\right)W(\vec{x}_\perp,\vec{k}_\perp;z,t) =\int d^2\vec{k}'_\perp\tilde{F}(\vec{k}_\perp-\vec{k}'_\perp)W(\vec{x}_\perp,\vec{k}'_\perp;z,t), \tag{4}$$

where

$$\tilde{F}(\Delta\vec{k}_\perp)=-v\mu_T\delta^2(\Delta\vec{k}_\perp)+\frac{vN}{k^2}\frac{d\sigma(\Delta\vec{k}_\perp)}{d\Omega}. \tag{5}$$

Here v is the speed of light inside the surrounding medium whose refraction index is n_0 ($v=c/n_0$), N is the number density of the scatterers, $k=2\pi n_0/\lambda$ is the magnitude of the wave vector, $(d\sigma/d\Omega)=|f(\Delta\vec{k}_\perp)|^2$ is the differential scattering cross section of a single scatterer for scattering from $\vec{k}'$ to $\vec{k}$ ($=\vec{k}'+\Delta\vec{k}_\perp$), and $f(\Delta\vec{k}_\perp)$ is the scattering amplitude of the scatterers. The total extinction coefficient μ_T is the sum of the absorption coefficient μ_A and the scattering coefficient μ_S. Note that the paraxial approximation, which allows $\tilde{F}(\vec{k}_\perp-\vec{k}'_\perp)$ to be expressed as a function of the difference of wave vectors, is applied in Eqs. (4) and (5). More general treatments can be found in Refs. [1,14,15].

A. Transport equation for near-forward scattering

Equations (4) and (5) are, in general, difficult to solve. However, if one considers the situation where the light field is predominantly scattered through only small angles by the random medium, then most of the scattered light propagates in the forward direction. This may be called generically near-forward scattering (snake-light scattering [17]). In this case one can assume, following the spirit of Ref. [9] that light scattered into large angles is weak compared to near-forward light, and the correlation between near-forward light and wide-angle light is weak. Then the WF of the total light field and the integral kernel can be separated into two parts:

$$W\approx W_N+\eta W^{(1)}, \tag{6}$$

$$\tilde{F}\approx\tilde{F}_N+\eta\tilde{F}^{(1)}, \tag{7}$$

where W_N and $\tilde{F}_N$ are the near-forward parts, η is a small perturbation parameter, and $W^{(1)}$ and $\tilde{F}^{(1)}$ are the first-order corrections corresponding to the wide-angle scattering. Thus Eq. (4) reads

$$\left(\partial_t+v\partial_z+\frac{v}{k}\vec{k}_\perp\cdot\vec{\nabla}_{\vec{x}\perp}\right)(W_N+\eta W^{(1)}) \approx\int d^2\vec{k}'_\perp(\tilde{F}_N+\eta\tilde{F}^{(1)})(W_N+\eta W^{(1)}). \tag{8}$$

The equation for terms of zero order in η is given by

$$\left(\partial_t+v\partial_z+\frac{v}{k}\vec{k}_\perp\cdot\vec{\nabla}_{\vec{x}\perp}\right)W_N=\int d^2\vec{k}'_\perp\tilde{F}_NW_N, \tag{9}$$

and the equation for terms of first order in η is given by

$$\left(\partial_t+v\partial_z+\frac{v}{k}\vec{k}_\perp\cdot\vec{\nabla}_{\vec{x}\perp}\right)W^{(1)} =\int d^2\vec{k}'_\perp\tilde{F}_NW^{(1)}+\int d^2\vec{k}'_\perp\tilde{F}^{(1)}W_N. \tag{10}$$

The angular range within which this approximation is valid is somewhat arbitrary, as long as it is sufficiently narrow. We find it convenient to define this angle as being equal to the collection angle of our optical system [18]. This angle is several times wider than the angular width of the main forward peak in the scattering cross section, for the type of medium we use (see below).

B. Gaussian approximation for the Mie scattering kernel

The near-forward part of the Mie differential scattering cross section shown in Fig. 1 can be approximated in the near-forward region by a Gaussian function with respect to the angle [9,19],

$$\left(\frac{d\sigma}{d\Omega}\right)_N\approx\frac{\sigma_N}{\pi\theta_0}\exp[-|\Delta\vec{k}|^2/(k^2\theta_0^2)], \tag{11}$$

where $|\Delta\vec{k}_\perp|=|\vec{k}_\perp-\vec{k}'_\perp|\approx k\sin\theta\approx k\theta$ is the magnitude of the change of transverse wave vector, and θ_0 (~ 5.8 mrad) is the $1/e$ half-width estimated from the Mie cross section (see Fig. 1) [20]. We take the integrated scattering cross section

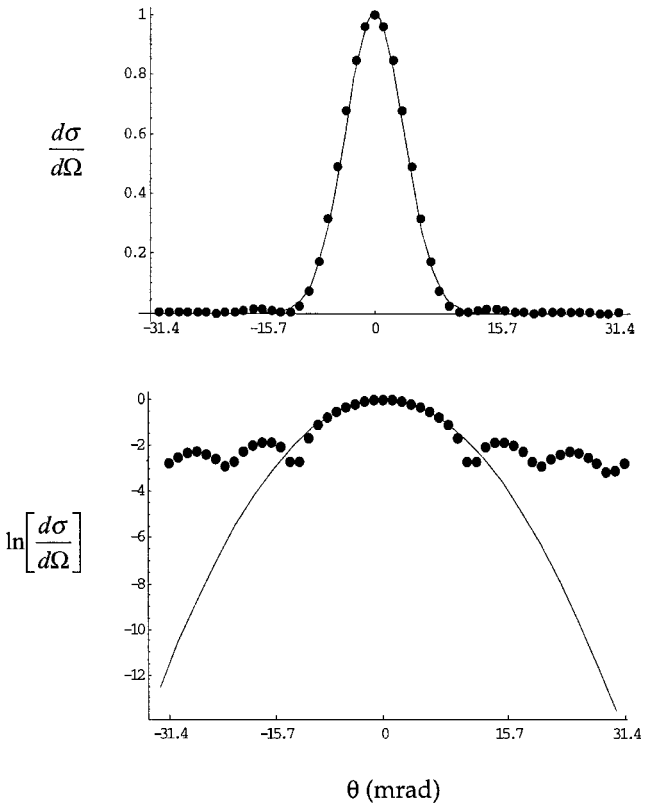

FIG. 1. Comparison of the Mie-theory differential cross section and its Gaussian approximation [Eq. (11)] for 46-μm-diam spheres with a refractive index $n=1.59$ in a medium with $n=1.42$. The circles are the Mie cross section, and the solid curves are its Gaussian approximation.

σ_N into the near-forward angles to be defined by the collection angle θ_C of our optical system,

$$\sigma_N \equiv \int_0^{2\pi} d\varphi \int_0^{\theta_C} d\theta \sin\theta \left(\frac{d\sigma}{d\Omega}\right)_{\mathrm{MIE}}, \tag{12}$$

where $(d\sigma/d\Omega)_{\mathrm{MIE}}$ is the Mie differential cross section. The normalization of $(d\sigma/d\Omega)_N$ reads

$$2\pi \int_0^{\infty} d\theta\, \theta \frac{\sigma_N}{\pi\theta_0} \exp[-\theta^2/\theta_0^2] = \sigma_N .$$

Fourier transforming Eq. (9) according to Eq. (2) yields

$$\left[\partial_z - \frac{i}{k}\vec{\nabla}_{\vec{x}_\perp}\cdot\vec{\nabla}_{\vec{s}_\perp} + \frac{1}{v}F_N(\vec{s}_\perp)\right]\Gamma_N(\vec{x}_\perp,\vec{s}_\perp,z) = 0, \tag{13}$$

where we considered the time-stationary case, and defined

$$\Gamma_N(\vec{x}_\perp,\vec{s}_\perp,z) \equiv \rho_N(\vec{x}_\perp+\vec{s}_\perp/2,\vec{x}_\perp-\vec{s}_\perp/2,z) = \langle E(\vec{x}_\perp+\vec{s}_\perp/2,z)E^*(\vec{x}_\perp-\vec{s}_\perp/2,z)\rangle, \tag{14}$$

and $F_N(\vec{s}_\perp)$ is the (minus of the) Fourier transform of $\tilde{F}_N(\Delta\vec{k}_\perp)$:

$$F_N(\vec{s}_\perp) = -\int d^2\vec{k}_\perp \exp[i\Delta\vec{k}_\perp\cdot\vec{s}_\perp]\tilde{F}_N(\Delta\vec{k}_\perp) = v\mu_T - vN\sigma_N \exp[-k^2\theta_0^2|\vec{s}_\perp|^2/4]. \tag{15}$$

Here we use Eq. (11) to evaluate $F_N(\vec{s}_\perp)$. Equation (13) establishes the fundamental wave-transport equation for the SCF.

To solve Eq. (13), we define a characteristic function

$$M(\vec{p},\vec{q},z) \equiv \left(\frac{1}{2\pi}\right)^4 \int d^2\vec{x}_\perp \int d^2\vec{s}_\perp \times \exp[-i\vec{p}\cdot\vec{x}_\perp - i\vec{q}\cdot\vec{s}_\perp]\Gamma_N(\vec{x}_\perp,\vec{s}_\perp,z). \tag{16}$$

Substituting Eq. (16) into Eq. (13), solving for $M(\vec{p},\vec{q},z)$, and then transforming back to Γ_N, one finds [21]

$$\Gamma_N(\vec{x}_\perp,\vec{s}_\perp,z) = \int d^2\vec{q} \exp[i\vec{q}\cdot\vec{x}_\perp] \times \exp\left[\frac{-1}{v}\int_0^z dz' F_N(\vec{s}_\perp - \vec{q}(z-z')/k)\right] \times \int \frac{d^2\vec{x}'_\perp}{(2\pi)^2} \exp[-i\vec{q}\cdot\vec{x}'_\perp] \times \Gamma_N(\vec{x}'_\perp,\vec{s}_\perp - \vec{q}z/k, z=0). \tag{17}$$

This is the general solution for Eq. (13), given the boundary condition for Γ_N at $z=0$:

$$\Gamma_N(\vec{x}_\perp,\vec{s}_\perp,z=0) = \langle E(\vec{x}_\perp+\vec{s}_\perp/2,z=0)E^*(\vec{x}_\perp-\vec{s}_\perp/2,z=0)\rangle. \tag{18}$$

Note that the wave-transport theory is not the only way to reach these predictions. For example, Eq. (17) can also be derived under the small-angle-scattering approximation by using the extended Huygens-Fresnel principle [22].

C. Model for optical transport experiments

In our experiments we used as the input light field a collimated Gaussian beam,

$$E(\vec{x}_\perp, z=0) = \left(\frac{1}{\pi a^2}\right)^{1/2} \exp[-|\vec{x}_\perp|^2/2a^2], \tag{19}$$

with normalization $\int d^2\vec{x}_\perp |E(\vec{x}_\perp,z=0)|^2 = 1$, and beam width $a = 140\,\mu$m. So the SCF of the input light is

$$\Gamma_N(\vec{x}_\perp,\vec{s}_\perp,0) = \frac{1}{\pi a^2}\exp\left[-\left(|\vec{x}_\perp|^2 + \frac{1}{4}|\vec{s}_\perp|^2\right)/a^2\right]. \tag{20}$$

Further, we rewrite Eq. (17) as

$$\Gamma_N(\vec{x}_\perp,\vec{s}_\perp,z)=\int d^2\vec{q}\,\exp[i\vec{q}\cdot\vec{x}_\perp]\times\exp[-I_1(\vec{s},\vec{q},z)]I_0(\vec{s},\vec{q},z), \quad (21)$$

where

$$I_1(\vec{s},\vec{q},z)=\frac{1}{v}\int_0^z dz' F(\vec{s}_\perp-\vec{q}(z-z')/k) = \mu_T z - N\sigma_N\int_0^z dz' \times\exp\left[-\frac{k^2\theta_0^2}{4}|\vec{s}_\perp-\vec{q}(z-z')/k|^2\right] \quad (22)$$

and

$$I_0(\vec{s},\vec{q},z)=\int\frac{d^2\vec{x}'_\perp}{(2\pi)^2}\exp[-i\vec{q}\cdot\vec{x}'_\perp]\Gamma_N(\vec{x}'_\perp,\vec{s}_\perp-\vec{q}z/k,z=0) = \frac{1}{(2\pi)^2}\exp\left[-\frac{|\vec{s}_\perp-\vec{q}z/k|^2}{4a^2}-\frac{a^2q^2}{4}\right]. \quad (23)$$

If we define the error function

$$\mathrm{erf}[x]\equiv\frac{2}{\sqrt{\pi}}\int_0^x dy\,\exp[-y^2],$$

which satisfies $\mathrm{erf}[0]=0$ and $\mathrm{erf}[\infty]=1$, then Eq. (22) reads

$$I_1(\vec{s},\vec{q},z)=\mu_T z-\frac{N\sigma_N\sqrt{\pi}}{\theta_0|\vec{q}|}\left\{\mathrm{erf}\left[\frac{k\theta_0}{2|\vec{q}|}\vec{q}\cdot\vec{s}\right]-\mathrm{erf}\left[\frac{k\theta_0}{2}(\vec{q}\cdot\vec{s}/|\vec{q}|-z|\vec{q}|/k)\right]\right\}. \quad (24)$$

In our experiments the optical field is sheared in one dimension, so we consider only $\vec{x}_\perp=(x,0,0)$ and $\vec{s}_\perp=(s,0,0)$. In this case, Eq. (21) reads (for $y=0$)

$$\Gamma_N(x,s,z)=\int dq\,\exp[iqx]\exp[-I_1(s,q,z)]I_0(s,q,z), \quad (25)$$

where

$$I_1(s,q,z)=\mu_T z-\frac{N\sigma_N\sqrt{\pi}}{\theta_0 q}\left\{\mathrm{erf}\left[\frac{k\theta_0}{2}s\right]-\mathrm{erf}\left[\frac{k\theta_0}{2}(s-zq/k)\right]\right\}, \quad (26)$$

and

$$I_0(s,q,z)=\frac{1}{2\pi}\exp\left[-\frac{(s-qz/k)^2}{4a^2}-\frac{a^2q^2}{4}\right]. \quad (27)$$

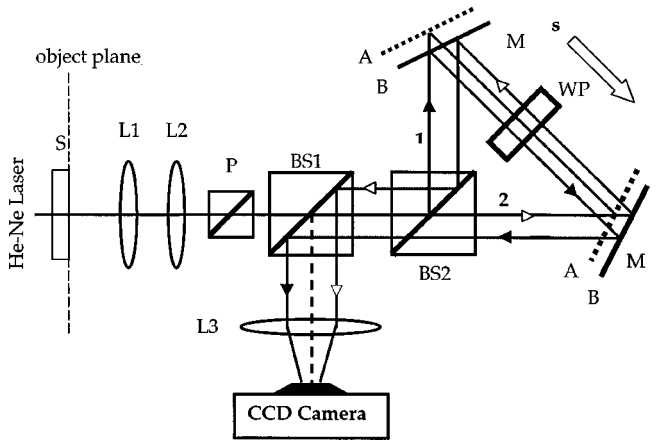

FIG. 2. The variable-shear Sagnac interferometer, which measures the spatial coherence function (SCF) of light emitted at the object plane. *S*, scattering medium or source. BS, nonpolarizing 50/50 beam splitters. *M*, mirror. *P*, polarizer. *L*, lens. WP, wave plate set.

Below we use Eqs. (25)–(27) to predict the SCF from the transport theory, and compare it with results from our experiments.

III. EXPERIMENTS AND COMPARISON WITH THEORY

A. High-numerical-aperture, variable-shear Sagnac interferometer

Figure 2 shows our experiment setup. Light from the sample or source (*S*) leaves the object plane, is collected by lenses $L1$ and $L2$, is linearly polarized by a polarizing cube (*P*), and passes through a nominal 50/50 nonpolarizing beam splitter (BS1) before entering the Sagnac interferometer through the second beam splitter (BS2). The light is equally split into clockwise- and counterclockwise-traveling beams, which undergo shears of equal magnitude, but opposite sign, before recombining at BS2, where interference takes place. After reflecting partially from BS1, the light is directed onto a charge-coupled device (CCD) camera, forming two overlapping images of the object plane, with interference fringes present. Interferograms are recorded and saved in computer memory. By varying the orientations of a set of intraring birefringent wave plates to introduce nonreciprocal phase shifts to the two counterpropagating beams, we perform measurements at four relative-phase values. From these four measurements we obtain the complex SCF [19,23]. Details of the design and operation of this wide-angle, variable-shear interferometer are given in our paper [23]. Our system is similar in layout to that of Iaconis and Walmsley [10], with modifications to increase the numerical aperture of the system without distorting the shape of the wave front and to avoid adding additional astigmatism.

We have tested the operation of the interferometer by measuring the SCF of a well-known coherent Gaussian beam from a laser. We find that the measured values of the SCF equal the expected values to within about 5–10 % of the peak value.

B. Spatial coherence function (SCF)

To study the spatial coherence function of light, we used a linearly polarized, continuous-wave He-Ne laser ($\lambda = 632.8$ nm) as the source of input light to a random medium composed of polystyrene microspheres (mean diameter 46 μm, standard deviation 0.64 μm, and refractive index $n = 1.59$ manufactured by Bangs Laboratories, Inc.), suspended in a solidified gelatin-water mixture ($n_0 = 1.42$) between two 1-mm-thick glass plates. See Fig. 2, in which the object plane is at the output surface of the medium, and is imaged onto the CCD camera. The ensemble averaging of spatial configurations defining the SCF was achieved by rapidly moving (at 15 Hz) the sample transversely over a range ± 5 mm while collecting data over a long exposure time (0.5 sec). The input light beam from the laser was collimated by a lens at the medium input face ($z = 0$) with a Gaussian-beam radius 140 μm (a half-width at $1/e$ maximum intensity).

To investigate how the coherence properties of the light change with depth into a medium, we keep the volume fraction (VF) of the microspheres in suspension at 2%, and change the thickness of the medium. The characteristics of a scattering medium with thickness L can be specified by the optical distance (OD), given by $\mathcal{O} = \mu_T L$, where μ_T $[= N(\sigma_A + \sigma_W + \sigma_N)]$ is the total extinction coefficient, with N being the number density of scatters (in this case $N = 3.9 \times 10^5\ \mathrm{cm}^{-3}$), and σ_N being the cross section integrated over near-forward angles, distinguished by being within the collection solid angle Ω_N of our optical system, as in Eq. (12). Likewise, σ_W is the cross section integrated over (wide) angles outside Ω_N. The total scattering cross section is σ_S $(= \sigma_N + \sigma_W)$. Other attenuation mechanisms, such as absorption, are represented by σ_A. The scattering cross section σ_S, calculated from Mie theory for this case, is $3.47 \times 10^{-5}\ \mathrm{cm}^2$, and the near-forward part of σ_S is σ_N $(= 0.68\sigma_S)$, which is determined by the collection solid angle of the optical system [24]. A contribution corresponding to 4% reflection from each glass plate holding the medium was included in σ_A [25]. We studied four cases—$L = 0.1$, 0.3, 0.5, and 1 cm—and the corresponding OD's at 2% VF are 1.34, 4.02, 6.70, and 13.4. In a nonabsorptive medium, $\mu_T \approx \mu_S$, where μ_S is the total scattering coefficient. The scattering mean free path is $l_S = (1/\mu_S)$. Then the OD of the medium (L/l_S) can be interpreted as the average number of scattering events occurring in the medium when light traverses it. A medium with an OD of 13.4 falls into the multiple-scattering regime, while a medium with an OD of 1.34 is close to a single-scattering regime.

The main difficulty of taking data in this experiment is to achieve a good ensemble average for a medium with large OD. We believe that this problem may be caused by the effects of the superposition of ballistic (unscattered) and scattered light, as discussed in the Appendix. We found that for thick media we needed to translate transversely the medium around several central locations over a range of 1 cm, and average the results from all of them to obtain a reasonable ensemble average (indicated by repeatability of results). For the medium with an OD of 13.4, we averaged over ten different central locations; for the medium with an OD of 6.70, we averaged over seven. But for the medium with OD's of 4.02 and 1.34, we just averaged over one fixed central location, and the resulting signal-to-noise ratio is acceptable.

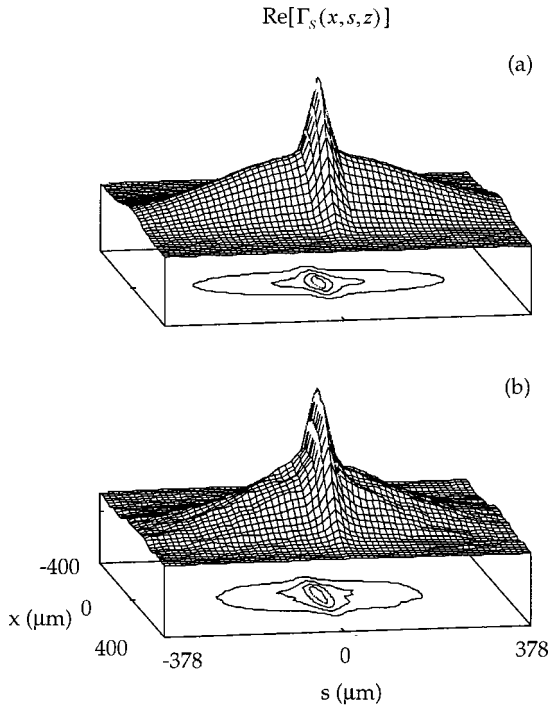

FIG. 3. The SCF for the optical distance $\mathcal{O} = 1.34$. (a) is the prediction of the theory [Eqs. (25)–(27)] for the real part of the SCF. (b) is the result of the experiment for the real part of the SCF.

Comparisons of the SCF of light obtained from theory and experiment are shown in Figs. 3–6. We use Γ_S to denote the measured SCF after scattering. The normalization of the SCF for both theory and experiment reads

$$1 = \int dx\, \Gamma(x, s=0, z) = \int dx\, \rho(x, x, z). \tag{28}$$

In theory, the imaginary part of the SCF of a collimated input beam, $\mathrm{Im}[\Gamma(x,s,z=0)]$, is zero. However, after our best efforts to collimate the laser beam, the SCF of the input still had a small imaginary part, with a relative magnitude

$$\left| \frac{\mathrm{Im}[\Gamma(x,s,z=0)]}{\mathrm{Re}[\Gamma(x,s,z=0)]} \right| \approx \frac{1}{40}.$$

In the cases of $\mathcal{O} = 1.34$ and 4.02, with an ideal input beam, Eqs. (25), (26), and (27) predict for this ratio at the output face of the medium,

$$\left| \frac{\mathrm{Im}[\Gamma_S(x,s,z)]}{\mathrm{Re}[\Gamma_S(x,s,z)]} \right| < \frac{1}{50},$$

where $\Gamma_S(x,s,z)$ is the SCF of the transmitted light. The measured SCF for the cases of $\mathcal{O} = 1.34$ and 4.02 gives

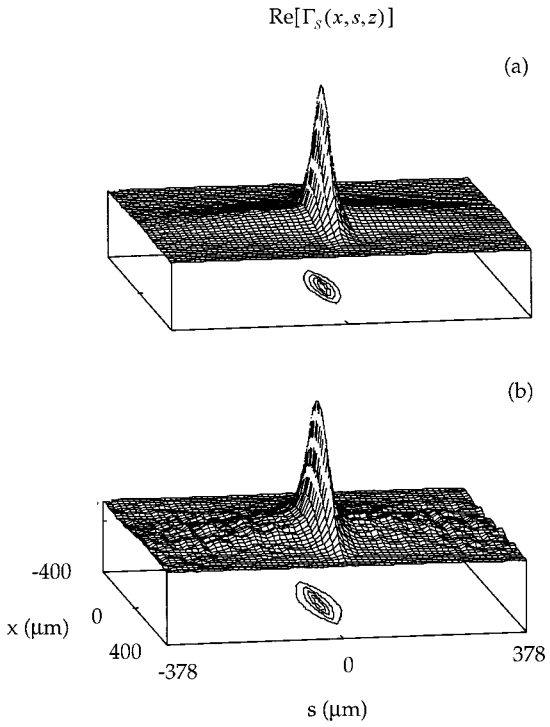

FIG. 4. The SCF for $\mathcal{O}=4.02$. (a) is the prediction of the theory [Eqs. (25)–(27)] for the real part of the SCF. (b) is the result of experiment for the real part of the SCF.

$$\left|\frac{\mathrm{Im}[\Gamma_S(x,s,z)]}{\mathrm{Re}[\Gamma_S(x,s,z)]}\right| \approx \frac{1}{30}.$$

They are essentially of the same order as the ratio

$$\left|\frac{\mathrm{Im}[\Gamma(x,s,z=0)]}{\mathrm{Re}[\Gamma(x,s,z=0)]}\right|$$

of the input beam, and we consider the measured $\mathrm{Im}[\Gamma_S]$ to be negligible in these two cases [26]. Therefore in Figs. 3 and 4, we show the real part of the SCF only, since we believe that it carries all of the essential physics.

In Fig. 3 we can see two distinctive components in the SCF from the side view in *s*-*x* space. Since the *s* range of the SCF is a measure of its transverse coherence length [27], the central narrow peak of the SCF corresponds to the partially coherent scattered light, whereas the broad component corresponds to the ballistic (unscattered) coherent component, which is proportional to the input SCF. As the OD of the medium increases in Figs. 4–6, the scattered light becomes stronger, while the ballistic light decays exponentially. When $\mathcal{O}\approx 5$, the scattered light dominates, and begins to look like a divergent Gaussian beam modulated by a narrow *s* width. This is, in fact, the physics behind the complex Gaussian-Schell model, as discussed later in this paper. The real part of the SCF in Fig. 6 for an OD of 13.4 is slightly diamond shaped; this shape is reminiscent of that observed in the SCF of a divergent coherent beam [19,23].

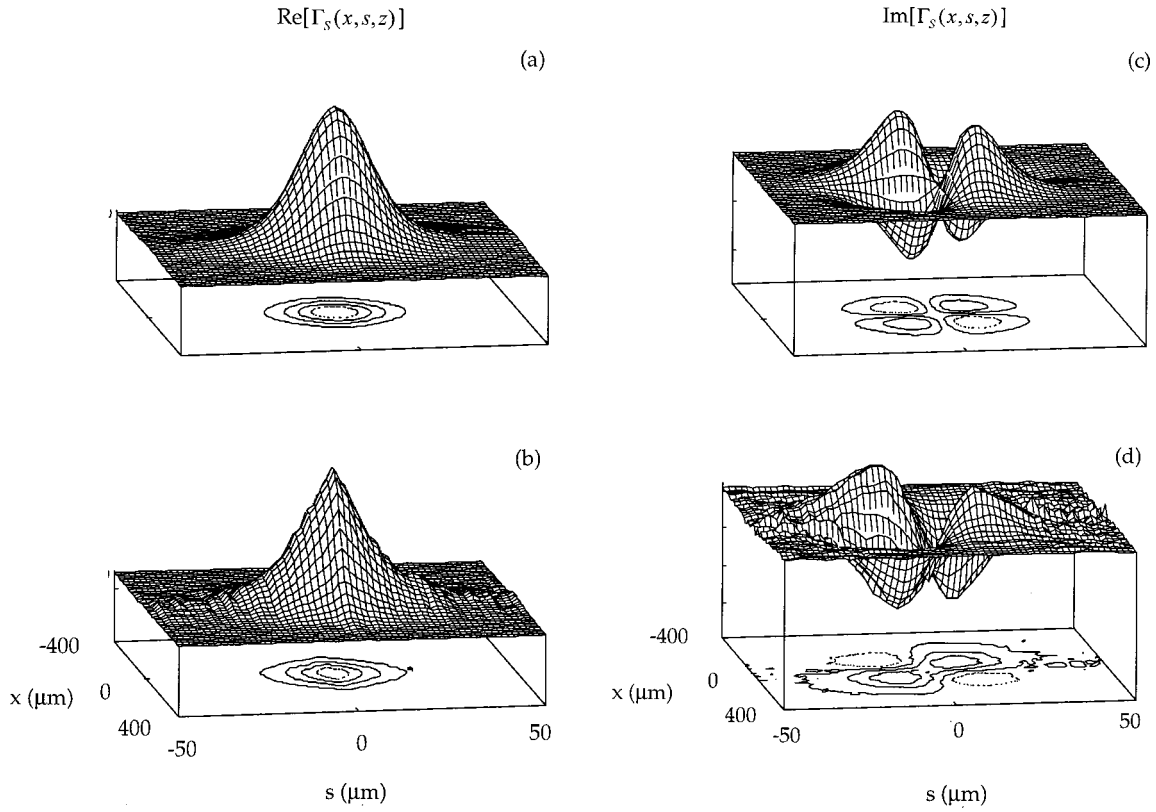

FIG. 5. The SCF for $\mathcal{O}=6.70$. (a) is the prediction of the theory [Eqs. (25)–(27)] for the real part of the SCF. (b) is the result of experiment for the real part of the SCF. (c) is the prediction of the theory for the imaginary part of the SCF. (d) is the result of experiment for the imaginary part of the SCF.

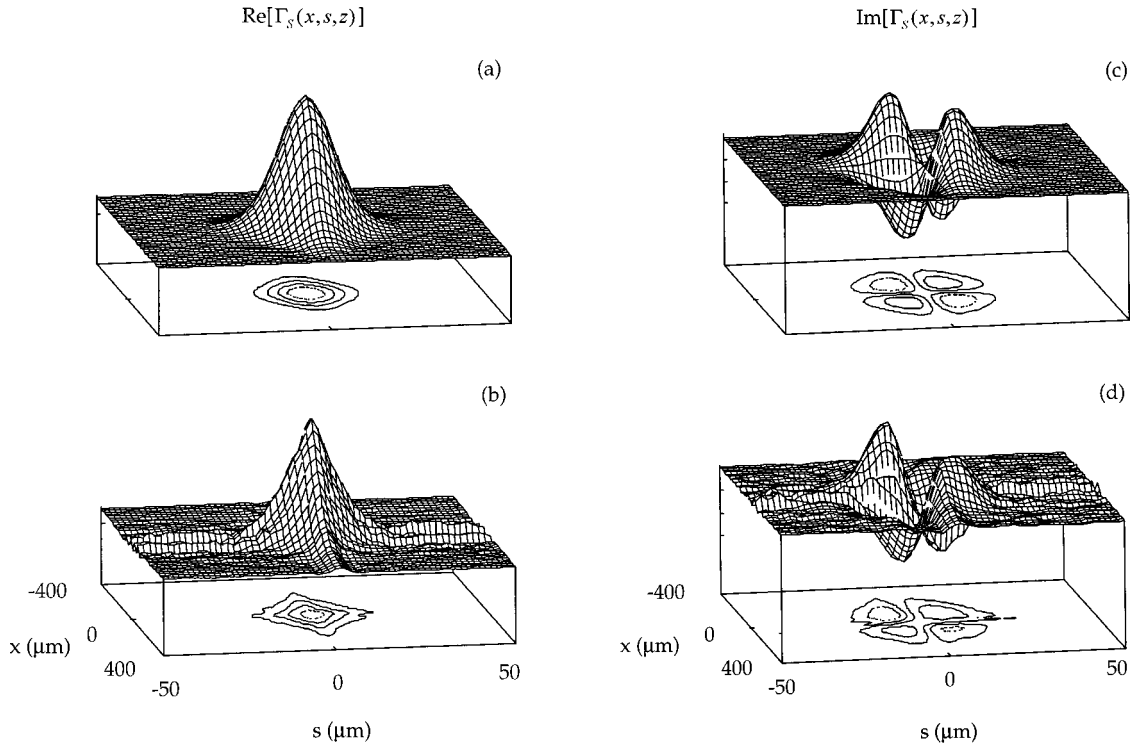

FIG. 6. The SCF for $\mathcal{O}=13.4$. (a) is the prediction of the theory [Eqs. (25)–(27)] for the real part of the SCF. (b) is the result of experiment for the real part of the SCF. (c) is the prediction of the theory for the imaginary part of the SCF. (d) is the result of experiment for the imaginary part of the SCF.

C. Wigner function

It is interesting to see how the Wigner function evolves from the case with a small OD to the case with a large OD, since the WF facilitates the visualization of the relation between the position and wave-propagation direction. The prediction for the WF corresponding to the above cases can be obtained numerically from Eq. (2) for the case of one-dimensional shear,

$$W_N(x,k,z)=\int \frac{ds}{2\pi}\exp[-isk]\Gamma_N(x,s,z), \qquad (29)$$

where $\Gamma_N(x,s,z)$ can be evaluated from Eqs. (25)–(27). In addition, the measured WF is obtained from the measured SCF by using a fast Fourier transform to evaluate Eq. (29). The results are shown in Figs. 7–10. The normalization of the WF from Eq. (28) reads

$$\int dx\,dk\,W_N(x,k,z)=1. \qquad (30)$$

The following interpretation for the WF is just opposite to the one for the SCF. The central peak of the WF in Figs. 7 and 8, which is narrow in k space, corresponds to the ballistic (unscattered) component of the light traversing the medium, whereas the broad peak corresponds to the scattered component. As the thickness of the medium increases, the ballistic light decays while the scattered light grows. When the OD reaches 6.70 the scattered light is dominant, and there is a significant spread of the WF in k space. Notice that the range of the k axis in Figs. 7 and 8 is about seven times smaller than the one in Figs. 9 and 10, indicating that the light spreads in k space significantly as the OD of the medium increases from 4.02 to 6.70. The contour of the WF in the case of $\mathcal{O}=13.4$ appears tilted, as is clearly shown in Fig. 11.

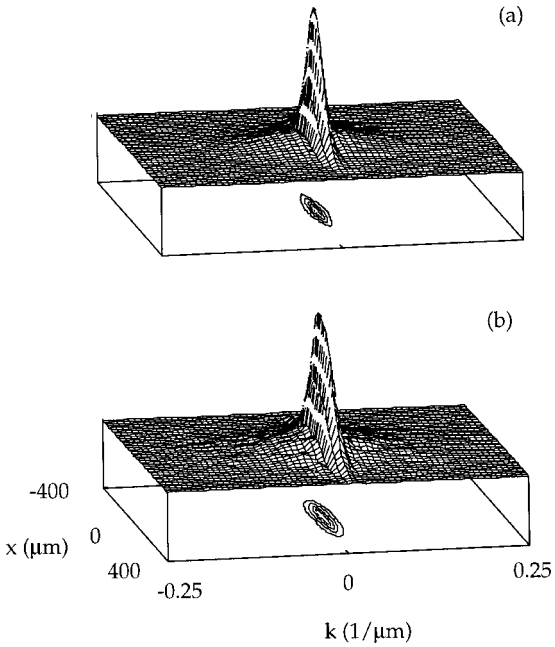

FIG. 7. The Wigner function (WF) for $\mathcal{O}=1.34$. (a) is the prediction of the theory [Eqs. (25)–(27) and (29)]. (b) is the result of experiment.

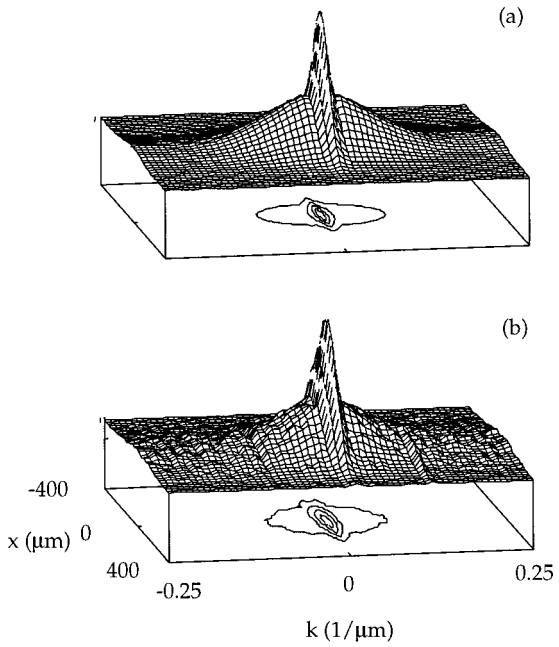

FIG. 8. The WF for $\mathcal{O}=4.02$. (a) is the prediction of the theory [Eqs. (25)–(27) and (29)]. (b) is the result of experiment.

This tilt (actually a shear) represents a divergent beam. The substantial agreement between our measurements and theory seen in Figs. 3–11 is, we believe, convincing evidence that the wave transport equation for the WF [Eq. (9)] provides an excellent description of near-forward wave transport in a random medium over a wide range of conditions.

IV. COMPLEX GAUSSIAN-SCHELL MODEL FOR NEAR-FORWARD SCATTERING LIGHT

As shown in previous sections, Eqs. (25)–(27) correctly model our experiments. To bring out the physics behind these equations, it may be interesting to consider a simple model as a qualitative guidance to explain the orders of magnitude of the quantities we measured. Here we show that strongly scattered light can be roughly modeled by a complex Gaussian-Schell model commonly used to describe partially coherent light.

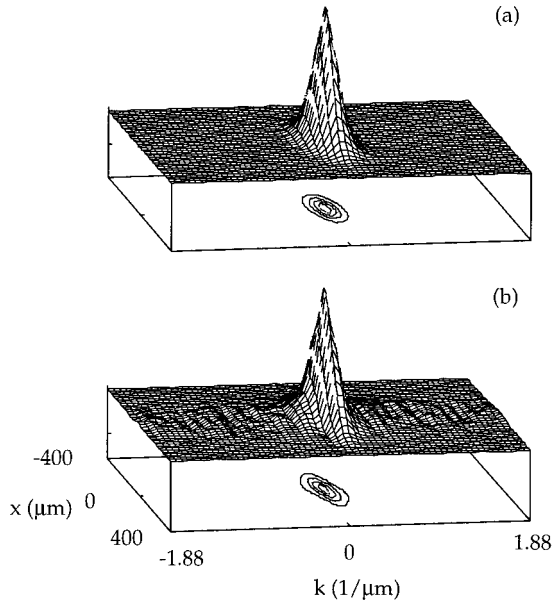

FIG. 9. The WF for $\mathcal{O}=6.70$. (a) is the prediction of the theory [Eqs. (25)–(27) and (29)]. (b) is the result of experiment.

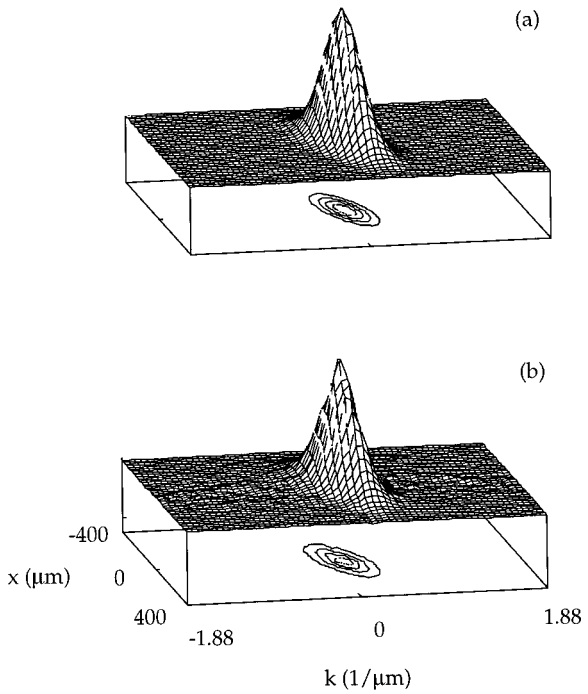

FIG. 10. The WF for $\mathcal{O}=13.4$. (a) is the prediction of the theory [Eqs. (25)–(27) and (29)]. (b) is the result of experiment.

Consider the strong-scattering case with large optical distance, e.g., $\mathcal{O}=13.4$. The SCF of the near-forward scattered light may be separated into two components,

$$\Gamma_N(\vec{x}_\perp,\vec{s}_\perp,z)\approx\Gamma_B(\vec{x}_\perp,\vec{s}_\perp,z)+\Gamma_{SC}(\vec{x}_\perp,\vec{s}_\perp,z), \quad (31)$$

where $\Gamma_B(\vec{x}_\perp,\vec{s}_\perp,z)$ is the ballistic (unscattered) part of the transmitted light, and $\Gamma_{SC}(\vec{x}_\perp,\vec{s}_\perp,z)$ is the scattered part. From Eq. (15) the scattering kernel can be written as

$$F_N(\vec{s}_\perp)=v\,\mu_T-v\,\mu_N\exp[-|\vec{s}_\perp|^2/s_0^2], \quad (32)$$

where $\mu_N(=N\sigma_N)$ can be interpreted as the near-forward scattering coefficient, and $s_0=2/k\theta_0$ is the $1/e$ half-width of the Fourier transform of the Gaussian approximation for the Mie cross section. It is reasonable to assume that $\Gamma_B(\vec{x}_\perp,\vec{s}_\perp,z)$ obeys [from Eqs. (13) and (15)]

$$\left(\partial_z-\frac{i}{k}\vec{\nabla}_{\vec{x}\perp}\cdot\vec{\nabla}_{\vec{s}\perp}+\mu_T\right)\Gamma_B(\vec{x}_\perp,\vec{s}_\perp,z)=0. \quad (33)$$

The solution of Eq. (33) can be approximated by [28]

$$\Gamma_B(\vec{x}_\perp,\vec{s}_\perp,z)\approx\exp[-\mu_T z]\Gamma_B(\vec{x}_\perp,\vec{s}_\perp,z=0). \quad (34)$$

Substituting Eqs. (31), (32), and (33) into Eq. (13) yields

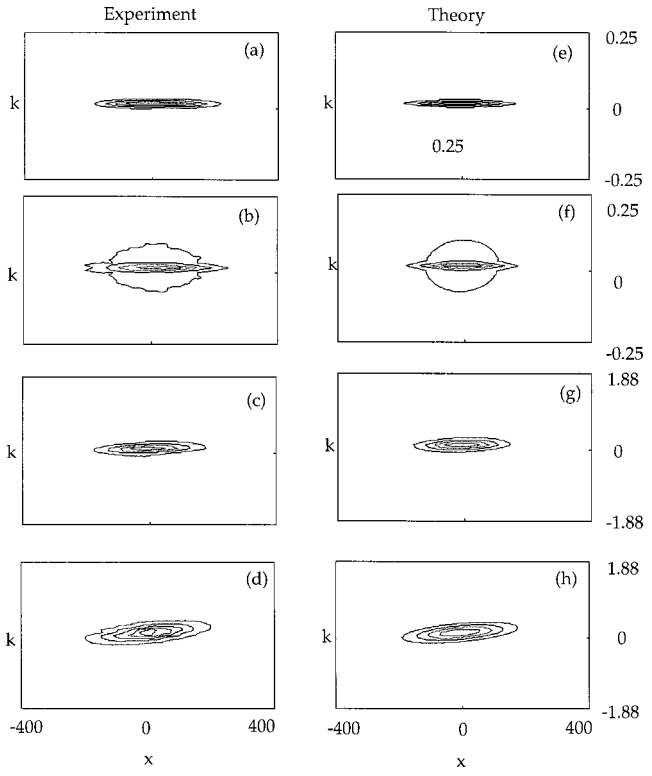

FIG. 11. Contour plots of the measured (predicted) WF for various optical distances. In (a) and (e), $\mathcal{O}=1.34$; in (b) and (f), $\mathcal{O}=4.02$; in (c) and (g), $\mathcal{O}=6.70$; and in (d) and (h), $\mathcal{O}=13.4$ [Units: x (μm) and k (μm)].

$$\left(\partial_z-\frac{i}{k}\vec{\nabla}_{\vec{x}_\perp}\cdot\vec{\nabla}_{\vec{s}_\perp}+\frac{1}{v}F_N(\vec{s}_\perp)\right)\Gamma_s(\vec{x}_\perp,\vec{s}_\perp,z)$$
$$-\mu_N\exp[-|\vec{s}_\perp|^2/s_0^2]\Gamma_B(\vec{x}_\perp,\vec{s}_\perp,z)=0. \quad (35)$$

Since $\mu_T L\gg 1$, in a rather crude approximation we treat the exponential function as a δ function, $\mu_T\exp[-\mu_T z]\approx\delta(z)$. So the last term in Eq. (35) can be approximated, by using Eq. (34), as

$$\mu_N\exp\left[-\frac{s^2}{s_0^2}\right]\Gamma_B(\vec{x}_\perp,\vec{s}_\perp,z)$$
$$\approx\mu_N\exp[-|\vec{s}_\perp|^2/s_0^2]\exp[-\mu_T z]\Gamma_B(\vec{x}_\perp,\vec{s}_\perp,z=0)$$
$$\approx\delta(z)B(\vec{x}_\perp,\vec{s}_\perp), \quad (36)$$

where

$$B(\vec{x}_\perp,\vec{s}_\perp)\equiv\frac{\mu_N}{\mu_T}\exp[-|\vec{s}_\perp|^2/s_0^2]\Gamma_B(\vec{x}_\perp,\vec{s}_\perp,z=0). \quad (37)$$

Now Eq. (35) becomes

$$\left(\partial_z-\frac{i}{k}\vec{\nabla}_{\vec{x}_\perp}\cdot\vec{\nabla}_{\vec{s}_\perp}+\frac{1}{v}F_N(\vec{s}_\perp)\right)\Gamma_{SC}(\vec{x}_\perp,\vec{s}_\perp,z)$$
$$=B(\vec{x}_\perp,\vec{s}_\perp)\delta(z), \quad (38)$$

with initial condition

$$\Gamma_{SC}(\vec{x}_\perp,\vec{s}_\perp,z=0)=0. \quad (39)$$

Equation (38) can be considered as a first-order differential equation in the z variable with a δ source. The solution of Eqs. (38) and (39) corresponds to the solution of the homogeneous equation

$$\left(\partial_z-\frac{i}{k}\vec{\nabla}_{\vec{x}_\perp}\cdot\vec{\nabla}_{\vec{s}_\perp}+\frac{1}{v}F_N(\vec{s}_\perp)\right)\Gamma_{SC}(\vec{x}_\perp,\vec{s}_\perp,z)=0, \quad (40)$$

with initial condition [see Eqs. (20) and (39)] given by

$$\Gamma_{SC}(\vec{x}_\perp,\vec{s}_\perp,z=0)=B(\vec{x}_\perp,\vec{s}_\perp)$$
$$=\frac{\mu_N}{\mu_T}\frac{1}{\pi a^2}$$
$$\times\exp\left[\frac{-|\vec{x}_\perp|^2}{a^2}-\left(\frac{1}{s_0^2}+\frac{1}{4a^2}\right)|\vec{s}_\perp|^2\right], \quad (41)$$

Equation (41) has a simple interpretation. At $z=0$, the scattered light is determined by the coherent input light [Eq. (20)], modulated by the factor $\exp(-|\vec{s}_\perp|^2/s_0^2)$. This factor will increase the exponential decay versus shear in Eq. (41), so the magnitude of the SCF, $|\Gamma_{SC}(\vec{x}_\perp,\vec{s}_\perp,z=0)|$, will become smaller than that of the SCF of the coherent input beam, $|\Gamma_B(\vec{x}_\perp,\vec{s}_\perp,z=0)|$. This indicates that the optical field loses most of its coherence almost immediately after the light leaves the plane $z=0$. Note that Eq. (41) is exactly the standard Gaussian Schell-model source, which is widely used for simple modeling of partially coherent light [5].

From Eq. (32), $F_N(\vec{s}_\perp)$ can be expanded in powers of s,

$$F_N(\vec{s}_\perp)=v\mu_\tau-v\mu_N[1-|\vec{s}_\perp|^2/s_0^2+\cdots]$$
$$=v\mu_W-v\Lambda|\vec{s}_\perp|^2+\cdots, \quad (42)$$

where $\mu_W\equiv\mu_T-\mu_N$ is the extinction coefficient resulting form wide-angle scattering, and $\Lambda\equiv\mu_N/s_0^2$. Next we assume the scattering is strong enough so Γ_{SC} is quite narrow in s space and all the features of interest are within the range of $s\sim s_0$ [29]. Then Eq. (40) can be approximated by

$$\left(\partial_z-\frac{i}{k}\vec{\nabla}_{\vec{x}_\perp}\cdot\vec{\nabla}_{\vec{s}_\perp}+(\mu_W-\Lambda|\vec{s}_\perp|^2)\right)\Gamma_{SC}(\vec{x}_\perp,\vec{s}_\perp,z)\approx 0. \quad (43)$$

For the case of one-dimensional propagation and shear $\vec{s}_\perp=(s,0,0)$, the solution of Eq. (43) with boundary condition (41) reads (for $y=0$) [30]

$$\Gamma_{SC}(x,s,z)=C_0(z)\exp[-\gamma(z)s^2]\exp\left[\frac{(ix+\beta(z)s)^2}{4\alpha(z)}\right], \quad (44)$$

where

$$\alpha(z)=\frac{\Lambda z^3}{3k^2}+\frac{z^2}{\eta^2k^2}+\frac{a^2}{4}, \quad (45)$$

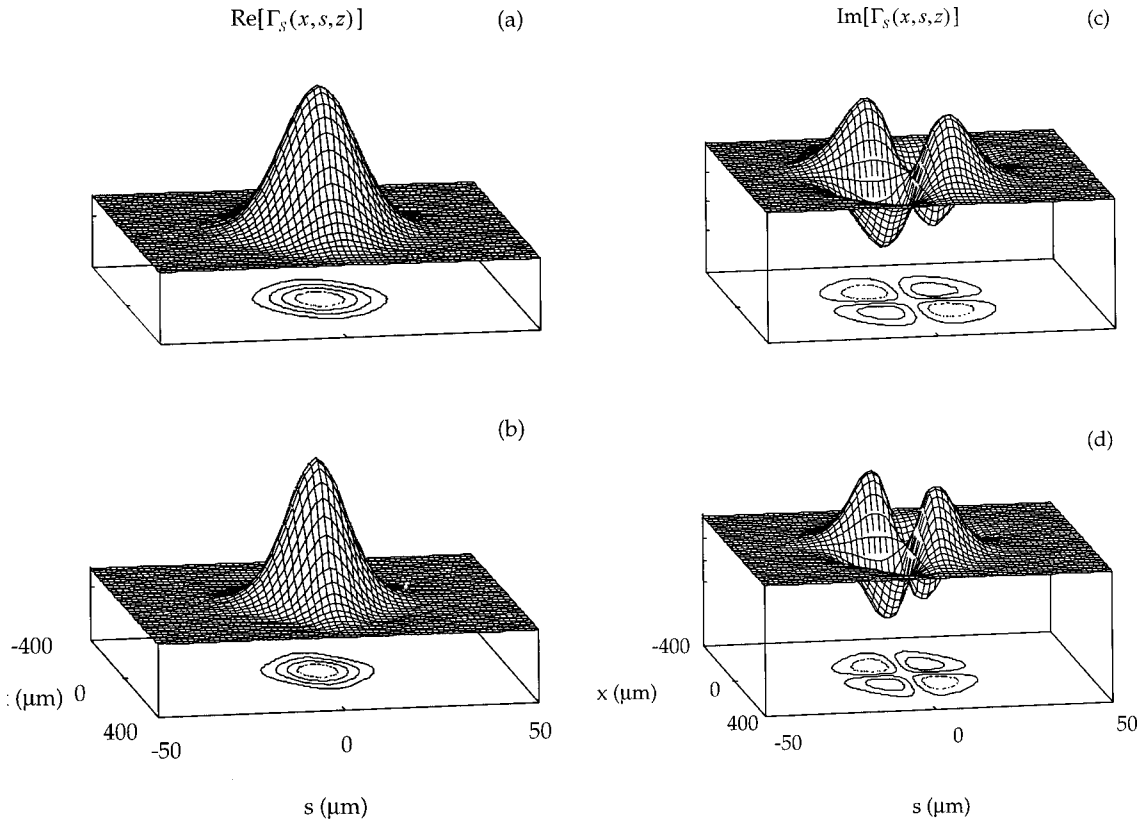

FIG. 12. Comparison between our simple analytical model and the transport model (for $\mathcal{O}=13.4$). (a) and (c) show the prediction, from our simple model [Eq. (44)] for the real part of the SCF. (b) and (d) show the prediction from the transport model [Eqs. (25)–(27)] for the imaginary part of the SCF.

$$\beta(z)=\left(\Lambda z+\frac{2}{\eta^2}\right)\frac{z}{k}, \tag{46}$$

$$\gamma(z)=\Lambda z+\frac{1}{\eta^2}, \tag{47}$$

$$\frac{1}{\eta^2}=\frac{1}{4a^2}+\frac{1}{s_0^2}, \tag{48}$$

and

$$C_0(z)=\frac{\mu_N}{2\mu_T}\left(\frac{1}{\pi\alpha(z)}\right)^{1/2}. \tag{49}$$

The normalized SCF predicted by this simple model [Eq. (44)], and the previous transport model [Eqs. (25)–(27)], are shown in Fig. 12 for comparison, for the case $\mu_T L=13.4$. They agree to within 20%, which means the approximations we used here are quite reasonable for describing the shape of the SCF of light traversing a thick, dense, near-forward scattering medium. The normalization used in Fig. 12 is according to Eq. (28).

However, we also found that the calculated prefactor $C_0(z=L)$ in this case ($\mu_T L=13.4$) is about ten times larger than the predicted value from the transport theory [Eqs. (25)–(27)]. This prefactor drops out in the normalized plots shown in Fig. 12. We believe that this discrepancy is caused by the crude approximation treating the source term in Eq. (35) as a δ function. This illustrates that this simple model [Eq. (44)] should be used only as a rough intuitive guide, and is not meant to replace the more accurate transport model of Eqs. (25)–(27).

V. DISCUSSION

The shapes of the SCF in Fig. 6 are somewhat similar to those for a divergent Gaussian beam with a large wave-front curvature [19]. This suggested that it may be possible to describe scattered light using a simpler model based on the functional form of a Gaussian beam with somewhat different parameters. This turned out to be the case. Equation (44), which we may call a complex Gaussian-Schell model (CGSM) for partially coherent light, has in fact been used previously to describe certain partially coherent optical fields propagating through a linear optical system [31]. We have just shown that this CGSM can be generalized to describe multiply scattered light without using free parameters, and still achieve reasonable agreement between theory and experiment.

The CGSM has a simple physical interpretation. For a strong, near-forward scattering medium, the coherent input beam loses most of its coherence almost right at the input plane at $z=0$ (after one mean free path), while the intensity profile of the light varies little. This leads to an effective input source, which is described by a CGSM source, Eq.

(41). The transverse coherence length of this effective source, on the order of $[(1/s_0^2)+(1/4a^2)]^{-1}$, has reduced the s range of interest to the order of $s_0(\ll a)$ [32] from the original range of the input beam $(\sim a)$. Then, for larger z, subsequent evolution of the scattered light can be described by Eq. (43), an approximate transport equation. In this equation we may identify $\mu_W-\Lambda|\vec{s}_\perp|^2$ as the rate of decorrelation of the field at two points spatially separated by a distance $|\vec{s}_\perp|$. This indicates that the decorrelation rate is minimal for nearby points, and increases quadratically with spatial separation. This behavior is closely analogous to the prediction in quantum theory, where decorrelation is referred to as decoherence [18,19].

The simplified transport equation for the Wigner function, according to Eqs. (2) and (43), is given by

$$\left(\partial_z+\frac{v}{k}\vec{k}_\perp\cdot\vec{\nabla}_{\vec{x}\perp}+\mu_W+\Lambda\vec{\nabla}^2_{\vec{k}\perp}\right)W(\vec{x}_\perp,\vec{k}_\perp,z)=0. \quad (50)$$

Equation (50) is a form of Fokker-Planck equation for diffusion of a transverse wave vector, including attenuation (μ_W) and the convective transport term $\vec{k}_\perp\cdot\vec{\nabla}_{\vec{x}\perp}$. The rate of wave-vector diffusion is $\Lambda\equiv\mu_N/s_0^2$. This indicates that the CGSM corresponds to the Fokker-Planck equation, a k-space diffusion approximation to the more complicated transport equation [Eq. (9)].

Our picture for the wave transport in a near-forward medium is thus the following. A coherent input beam enters the medium, and after one mean free path its intensity profile varies little, whereas its SCF rapidly evolves into that of a CGSM. Since the coherence length is now quite small, the proper transport equation can be replaced by Eqs. (43) or (50), in which further decorrelation and intensity evolution is modeled simply by a diffusion of transverse wave vector. Note that this behavior is distinct from spatial diffusion.

In summary, our experiments verify that the proposed wave-transport equation (4) provides a quantitative description of the evolution of the second-order spatial coherence of light in a random multiple-scattering medium in the near-forward scattering regime. Further experiment and theory are needed to explore the case of a medium with stronger wide-angle scattering, as in certain biotissues, for example.

ACKNOWLEDGMENTS

We thank H. Heier for collaboration on the interferometer design, and S. Jacques for support and collaboration. This work was supported by the U.S. Army Research Office and by the DOE through the Oregon Medical Laser Center.

APPENDIX

A speckle pattern can be caused by the self-interference of narrow-band, thermal-like (i.e., blackbody) light described by Gaussian field statistics. The probability distribution (histogram) for the intensity of narrow-band, thermal light is a negative-exponential distribution, so the most probable value for intensity in this case is zero. In contrast, it has been established that the superposition of coherent and thermal light will have a different intensity probability histogram [33]. In this case the probability of obtaining zero intensity is decreased compared to that in the case of pure thermal light, which is caused by the nonzero mean amplitude of the coherent component. In our experiments the coherent component is the unscattered input light, while the thermal-like component is the light scattered in the medium. Their superposition makes it difficult to average out certain particular medium configurations by a limited-range uniaxial movement. Further discussion can be found in Ref. [19].

[1] S. John, G. Pang, and Y. Yang, J. Biomed. Opt. **1**, 180 (1996).
[2] H. H. Natsuyama, S. Ueno, and A. P. Wang, *Terrestrial Radiative Transfer* (Springer, New York, 1998).
[3] See, for example, E. Kohen, R. Santus, and J. G. Hirschberg, *Photobiology* (Academic, San Diego, 1995).
[4] V. V. Sobolev, translated by S. I. Gaposchkin, *A Treatise on Radiative Transfer* (Van Nostrand, New York, 1963); B. V. Komberg, A. V. Kravtsov, and V. N. Lukash, Astron. Astrophys. **286**, L19 (1994).
[5] L. Mandel and E. Wolf, *Optical Coherence and Quantum Optics* (Cambridge University Press, New York, 1995).
[6] A. Ishimaru, *Wave Propagation and Scattering in Random Media* (Academic, New York, 1978), Vol. II.
[7] A. Walther, J. Opt. Soc. Am. **58**, 1256 (1968); Yu. A. Kravtsov and L. A. Apresyan, in *Progress in Optics XXXVI*, edited by E. Wolf (North-Holland, Amsterdam, 1996), p. 179.
[8] For a review, see P. Sheng, *Introduction to Wave Scattering, Localization and Mesoscopic Phenomena* (Academic, San Diego, 1995).
[9] A. Wax and J. E. Thomas, J. Opt. Soc. Am. A **15**, 1896 (1998).
[10] C. Iaconis and I. A. Walmsley, Opt. Lett. **21**, 1783 (1996).
[11] D. McAlister, M. Beck, L. Clarke, A. Mayer, and M. G. Raymer, Opt. Lett. **20**, 1181 (1995).
[12] R. F. Lutomirski and H. T. Yura, Appl. Opt. **10**, 1652 (1971).
[13] H. T. Yura, Appl. Opt. **11**, 1399 (1972).
[14] J. E. Thomas (private communication).
[15] L. Ryzhik, G. Papanicolaou, and J. B. Keller, Wave Motion **24**, 327 (1996).
[16] Early literature, e.g., D. Arnush, J. Opt. Soc. Am. **62**, 1109 (1971), mentioned that the (generalized) radiance obeys a transport equation under a small-angle-scattering approximation, although it is not clear from this context whether this transport equation is based on wave transport or energy (specific intensity) transport.
[17] L. Wang, P. P. Ho, C. Liu, G. Zhang, and R. R. Alfano, Science **253**, 769 (1991).
[18] Chung-Chieh Cheng and M. G. Raymer, Phys. Rev. Lett. **82**, 4807 (1999), and references therein.
[19] Chung-Chieh Cheng, Ph.D. dissertation, University of Oregon, 1999.

[20] This approximation for the Mie scattering cross section may not be accurate for the behaviors of the SCF around $s=0$. See Refs. [18] and [19].

[21] A. Ishimaru, *Wave Propagation and Scattering in Random Media* (Ref. [6]), Chap. 20.

[22] H. T. Yura (private communication) (unpublished); in *Union Radio Scientifique Internationale, Open Symposium, La Baule, Loire-Atlantique, France, 1977* (Comité National Francais de la Radio-electricité Scientifique, Issy-les-Moulineaux, France, 1977), pp. 65–69.

[23] Chung-Chieh Cheng, M. G. Raymer, and H. Heier, J. Mod. Opt. **47**, 1237 (2000).

[24] The collection solid angle can be written as $\Omega_N=2\pi(1-\cos\theta_C)$. Ray tracing our optical system to find the collection half angle θ_C yields a range of 0.10–0.15 rad, depending on the assumed spatial distribution of the scatterers within the laser beam. The results of theory are not highly sensitive to the precise value used; we use $\theta_C=0.14$ rad.

[25] $96\%\sim e^{-0.04}$ of light enters the medium without being reflected by the glass plate, so we use $N\sigma_A L=0.04$.

[26] We calculated the WF and found that the imaginary parts of the SCF in these two cases do not cause any appreciable change in the resulting WF, compared to the case in which we replaced the measured $\mathrm{Im}[\Gamma_S]$ by zero.

[27] For an incoherent field, $\Gamma_N(x,s,z)\sim I(x,z)\,\delta(s)$, where $I(x,z)$ is the intensity of the field. This clearly indicates that $\Gamma_N=0$ except at $s=0$, meaning there is no correlation between any two distinct spatial field points.

[28] The diffraction effect from free-space propagation of a collimated Gaussian beam over a distance $1/\mu_T$ is not strong, so in this approximation we neglect the diffraction term $(\nabla_{\vec{x}\perp}\cdot\nabla_{\vec{s}\perp})$.

[29] A detailed analysis, based on integrating Eq. (40) neglecting the diffractive derivative, shows that this is valid when $\mu_N z\gg 1$.

[30] Equation (44) is most easily obtained by evaluating the general solution [Eqs. (25)–(27)] in the special case under consideration.

[31] R. Simon, E. C. G. Sudarshan, and N. Mukunda, Phys. Rev. A **29**, 3273 (1984).

[32] For a sphere of diameter 46 μm, $s_0\sim 25\,\mu$m. The input Gaussian beam radius (the half-width of the $1/e$ maximum intensity) is $a=140\,\mu$m.

[33] See, for example, B. Saleh, *Photoelectron Statistics* (Springer-Verlag, New York, 1978), pp. 123–128.